Proceedings World Geothermal Congress 2026
Calgary, Canada, June 8 – 11, 2026

Testing Geothermal Hypotheses Beneath Corbetti, Ethiopia, with 3D S-wave Seismic Tomography

Ruiyi Yang[1], Brandon VanderBeek[1], Sebastian Rost[1], Andy Nowacki[1]*
[1]School of Earth and Environment, University of Leeds, UK
*a.nowacki@leeds.ac.uk

Keywords: Corbetti, Ethiopia, seismic tomography, seismicity

ABSTRACT

Seismic data can be used to constrain physical properties in and beneath geothermal reservoirs, but this relies on favorable ambient noise or a supply of natural earthquakes as sources. These may not always be available. We present the results of seismic shear-wave velocity tomography at Corbetti, a geothermal prospect in the Main Ethiopian Rift, using a limited catalogue of data to demonstrate the utility of probabilistic approaches which provide reliable uncertainties and prevent over-interpretation of particular model features. We find weak evidence to support a cross-rift structure which controls the shallow (<1 km depth) subsurface, but a stronger requirement for a deeper (~6 km) low-velocity feature which may be the top of the volcano's magmatic source.

1 INTRODUCTION

Corbetti lies in the central Main Ethiopian Rift (Figure 1) and has been the site of extensive study for geothermal development for several decades (Altaye et al., 1986; Paola, 1971). A number of recent geophysical studies have attempted to infer the causes of deformation observed from satellite and gravity data (Dualeh and Biggs, 2025; Gottsmann et al., 2020; R Lloyd et al., 2018; Wassihun et al., 2026), while geochemical and geological studies have examined magma generation and storage deeper beneath the volcano (Colby et al., 2024, 2022). Despite this, there has thus far been no attempt to image the elastic (seismic) structure beneath Corbetti. This is important, because constraining properties such as porosity, fluid saturation, fluid composition and temperature requires complementary measures of different physical properties. In this study we present a seismic shear wave analysis of the elastic structure beneath Corbetti from a limited dataset of seismic travel times, using probabilistic approaches that allows us to interrogate the uncertainties present in the structure.

2 DATA AND METHODS

2.1 Seismic network and local earthquake catalog

The Y6 network of 18 broadband three-component seismometers recorded continuously between 2016 and 2017 in the study area. These stations have previously been used to create a catalog of 122 local earthquakes up to a maximum magnitude of 4.2 (Lavayssière et al., 2019; Figure 1). This showed that while there is significant seismicity in the Hawassa area, two clusters of seismicity lie beneath the edges of the Chabbi and Urji edifices within Corbetti (Figure 1) at depths to 10 km below sea level (bsl). The initial catalog includes 1307 S-wave arrival time picks; we discard those stated to have a pick error larger than 0.02 s, leaving 424 high-quality travel times.

This does not represent a very large number of arrivals with which to perform traditional seismic tomography, but for the purposes of this study we are interested in how well tomography can be undertaken with such limited data and leave enhancement of the catalog to future work. Encouragingly, in our final catalog, seismicity is not confined to the shallowest depths (e.g., < 2 km) nor only the center of the caldera (Figure 2), meaning we expect some coverage of both the putative geothermal reservoir and deformation sources.

The reference 1D S-wave velocity model is taken from Lavayssière et al. (2019), where we convert the P-wave model to S-wave velocity using their ratio of P- to S-wave velocity $V_P/V_S = 1.683$.

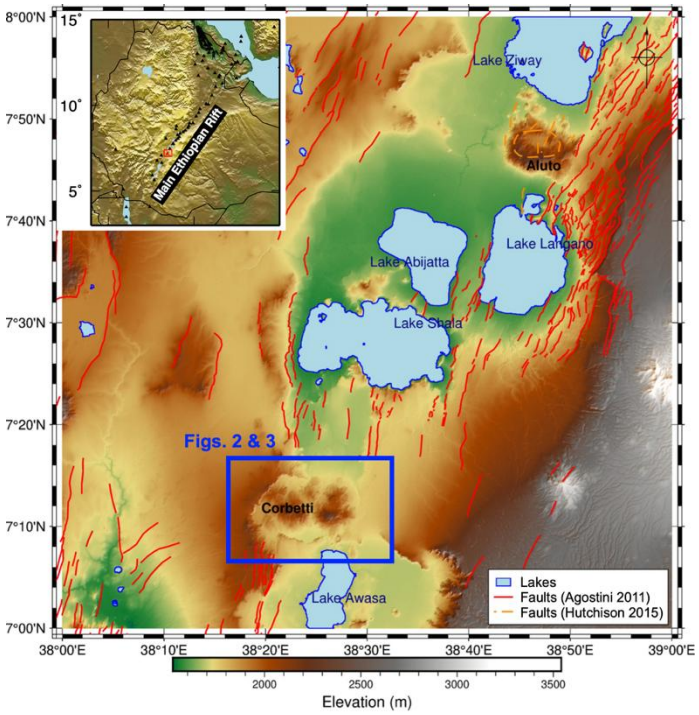


Figure 1. Overview of the Main Ethiopian Rift (inset) and region around Corbetti. The inset shows the location of the main figure. Faults from Agostini et al. (2011) and Hutchison et al. (2015) are shown. Black triangles in inset are volcanoes.

2.2 Seismic velocity tomography inference

Traditional seismic tomography typically is aimed at finding a single best-fitting model of wave velocity which matches the data (e.g., Bodin and Sambridge, 2009). However these methods have drawbacks: there are rarely formal estimates of uncertainty in the model parameters; they may strongly depend on the initial velocity model at the start of the inversion; and the parameterization of the model must be pre-determined and may affect the result. Therefore we choose to use a Bayesian method which gives an estimate of the posterior probability that any point in the model takes a certain value (Bodin and Sambridge, 2009; Zhang et al., 2020), given the data and our prior knowledge. In particular, we use the PSI_S approach (Del Piccolo et al., 2024) which makes use of the reversible-jump Markov chain Monte Carlo (rj-McMC) method to generate an ensemble of models which fit the data about equally well, and whose distribution approximates the posterior probability. Our implementation allows the data to determine the parametrization of the model because this is also updated as a set of hyperparameters in the inference procedure. (For full details of the method, see Del Piccolo et al., 2024.)

We infer the deviation from the background 1D model of the local S-wave velocity $\mathrm{d}\ln V_S = \ln(V_S/V_{S^{\mathrm{ref}}})$, where V_S is the local S-wave velocity and $V_{S^{\mathrm{ref}}}$ is the reference velocity at that depth. We impose a uniform prior of $\mathrm{d}\ln V_S$ between –0.4 and 0.4 (*i.e.*, –32% to 50% change relative to the background). We construct 84 parallel MC chains each of length 10^7 samples, and retain 1 in every 10^5 models to avoid strong correlations between samples in the chain. Finally, we discard the first 75% of samples to ensure sampling convergence. The final ensemble contains 2184 realizations of V_S models compatible with the data, which we examine in the following sections.

3 RESULTS AND INTERPRETATION

Figure 2 shows the uncertainty in the ensemble at a depth of 1 km bsl. We estimate the uncertainty by showing the width of the distribution between the 5$^{\mathrm{th}}$ and 95$^{\mathrm{th}}$ centile; *i.e.*, the range within which there is a 90% probability that the true value lies, given our prior constraint. This shows that in many parts of the model, this range encompasses the entire prior, meaning the data do not place a strong constraint on the inferred V_S structure. From here on, we mask out regions of the model where the 90% range is wider than 0.2 unless stated, leaving only regions where we can be more certain that they represent variations in S-wave velocity.

Figure 3 shows the median $\mathrm{d}\ln V_S$ values, at various depths in the model. The strongest feature is that the median is almost always faster than the reference 1D model. This may be because the velocity in this part of the caldera is overall faster than previously found for the wider Hawassa region by Lavayssière et al. (2019), or may reflect strong lateral variations in V_P/V_S. In either case, we do not seek to interpret the absolute velocity, but rather the spatial variation in $\mathrm{d}\ln V_S$.

At shallow depths (down to ~1 km bsl), there is a contrast between higher velocities in the center of the caldera and lower velocities to the north. This matches closely with the cross-rift structure seen by multiple previous studies in the conductivity structure (Figure 4; Dambly et al., 2024; Gíslason et al., 2015) and geodetic observations (Dualeh and Biggs, 2025; Gottsmann et al., 2020; R Lloyd et al., 2018; Ryan Lloyd et al., 2018). Previous studies have suggested this is caused by a cross-caldera structure constraining the hydrothermal system in the top few km, leading to lateral variations in uplift and conductivity.

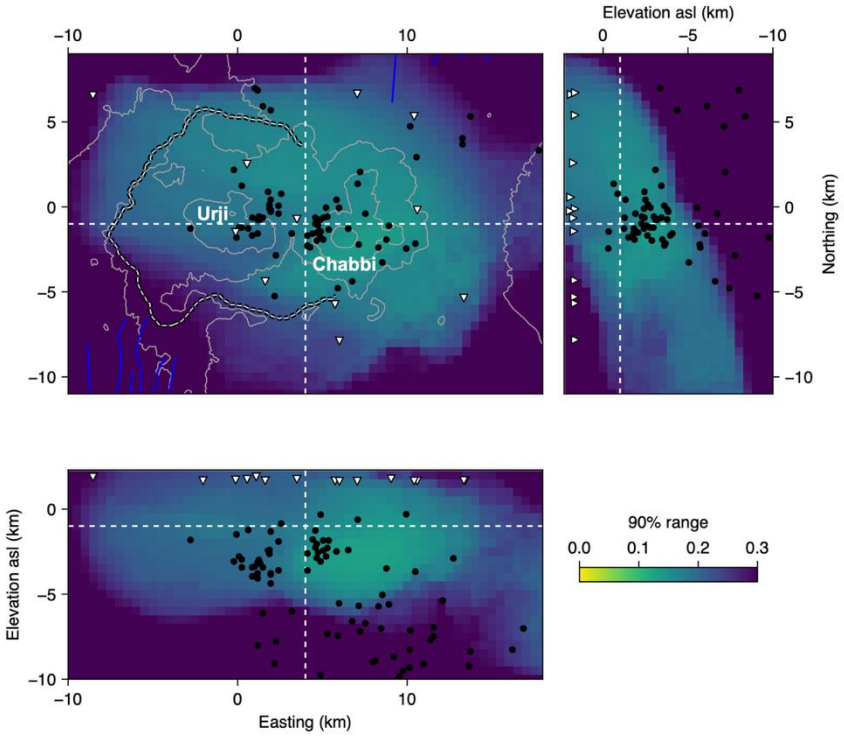


Figure 2. Uncertainty in the ensemble of $\mathrm{d}\ln V_S$ models at 1 km below sea level (bsl), shown by the difference between the 5th and 95th centiles at each point in the model space. White dashed lines show the line of the sections; also shown are seismic stations (inverted white triangles), earthquake locations (black circles; Lavayssière et al., 2019) and mapped faults (Agostini et al., 2011). The visible caldera rim is the black and white dashed line; topography contours each 200 m are in gray. Local eastings, northings and elevation are relative to WGS84 longitude 38.38°E and latitude 7.2°N. Chabbi and Urji are indicated.

4 DISCUSSION AND CONCLUSIONS

We have performed the first seismic velocity tomography beneath Corbetti, a geothermal prospect in the central Main Ethiopian Rift. We show that the seismic data favors a low-velocity body at ~5 km bsl beneath the east-central part of the caldera, agreeing with previous geodetic and gravity studies. This corroborating evidence supports the hypothesis that heat and surface deformation are focused beneath Urji at present, further constraining the magmatic origin of the system. Although currently the available seismic data are limited, it may be possible to further constrain the model in a number of ways, including expanding the seismic catalog with novel earthquake detection procedures (e.g., Shi et al., 2022) and making use of ambient noise to obtain surface wave dispersion measurements between pairs of stations (e.g., Shapiro and Campillo, 2004; Zhang et al., 2020). In any case, we expect future work to allow seismic data to help prove or disprove hypotheses about the processes occurring beneath one of Ethiopia's most important geothermal prospects.

Acknowledgements

We are grateful to Aude Lavayssière and Derek Keir for providing the seismic catalog and phase picks used in this study, and to Derek Keir for discussions. BVB and AN were funded by Geosolutions Leeds (project 'Testable geophysical and geological models from probabilistic imaging'). AN was also funded by NERC (grant NE/T012684/1). SR was partly funded by NERC (grant NE/Z00036X/1). The code used to perform the inference in this work is available at https://github.com/bvanderbeek/PSI_S.

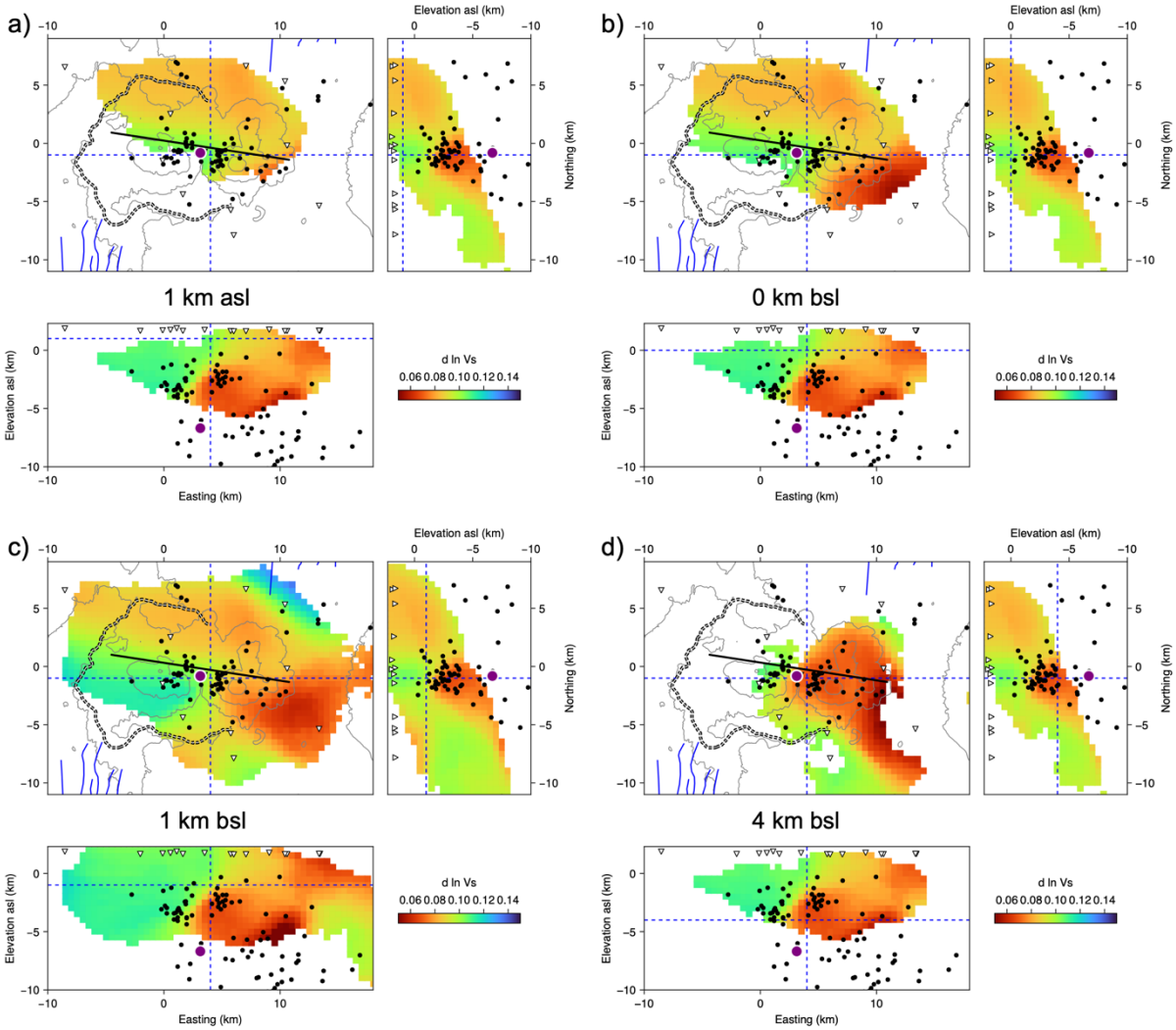


Figure 3. Median values of $\mathrm{d}\ln V_S$, the relative perturbation of S-wave velocity beneath Corbetti compared to the 1D reference model. Sections are shown at (a) 1 km above sea level (asl), (b) sea level, (c) 1 km below sea level (bsl) and (c) 4 km bsl. The solid black line shows the inferred boundary between the north and south of the caldera based on resistivity and ground motion (Dualeh and Biggs, 2025; Gíslason et al., 2015; R Lloyd et al., 2018), and the purple circle shows the position of the Mogi model of Dualeh and Biggs (2025). Other features as for Figure 2.

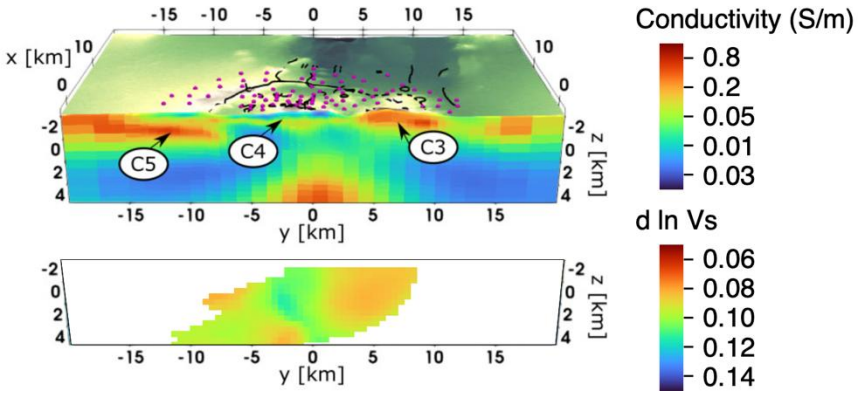


Figure 4. South (left) to north (right) cross-section through (top) the conductivity model of Dambly et al. (2024) and (bottom) our model of S-wave velocity anomaly, masked with a maximum 90% range of $\mathrm{d}\ln V_S$ of 0.25. Where resolved, the seismic model corroborates the MT-derived structure with a high V_S (low-conductivity) region beneath the center of the caldera and a slower (high-conductivity) region to the north at y = 5 km. There is a hint of a low-V_S region corresponding to the C5 anomaly to the south. Modified from Figure 4 of Dambly et al. (2024).

REFERENCES

Agostini, A., Bonini, M., Corti, G., Sani, F., Mazzarini, F.: Fault architecture in the Main Ethiopian Rift and comparison with experimental models: Implications for rift evolution and Nubia–Somalia kinematics. *Earth and Planetary Science Letters,* **301** (2011), 479–492. https://doi.org/10.1016/j.epsl.2010.11.024

Altaye, E., Befekadu, O., Hunegnaw, A., Tadesse, K., Abdulkadir, M., Mohammedberhan: A Review of Geological and Geophysical Exploration of Corbetti Geothermal Prospect, Ethiopia, in: *Proceedings*, 8th New Zealand Geothermal Workshop, New Zealand (1986), pp. 205–211.

Bodin, T., Sambridge, M.: Seismic tomography with the reversible jump algorithm. *Geophysical Journal International* **178** (2009), 1411–1436. https://doi.org/10.1111/j.1365-246X.2009.04226.x

Colby, D.J., Pyle, D.M., Fontijn, K., Mather, T.A., Melaku, A.A., Mengesha, M.A., Yirgu, G.: Stratigraphy and eruptive history of Corbetti Caldera in the Main Ethiopian Rift. *Journal of Volcanology and Geothermal Research* **428** (2022), 107580. https://doi.org/10.1016/j.jvolgeores.2022.107580

Colby, D.J., Pyle, D.M., Fontijn, K., Mather, T.A., Nomade, S., Melaku, A.A., Mengesha, M.A., Yirgu, G.: Magma storage conditions beneath a peralkaline caldera in the Main Ethiopian Rift. *Journal of Volcanology and Geothermal Research* **455** (2024), 108165. https://doi.org/10.1016/j.jvolgeores.2024.108165

Dambly, M.L.T., Samrock, F., Grayver, A., Eysteinsson, H., Saar, M.O.: Geophysical imaging of the active magmatic intrusion and geothermal reservoir formation beneath the Corbetti prospect, Main Ethiopian Rift. *Geophysical Journal International* **236** (2024), 1764–1781. https://doi.org/10.1093/gji/ggad493

Del Piccolo, G., VanderBeek, B.P., Faccenda, M., Morelli, A., Byrnes, J.S.: Imaging upper-mantle anisotropy with transdimensional Bayesian Monte Carlo sampling. *Bulletin of the Seismological Society of America* **114** (2024), 1214–1226. https://doi.org/10.1785/0120230233

Dualeh, E.W., Biggs, J.: Separating magmatic and hydrothermal deformation using InSAR timeseries: Independent component analysis at Corbetti caldera, Ethiopia. *Journal of Geophysical Research: Solid Earth* **130** (2025), e2024JB030974. https://doi.org/10.1029/2024JB030974

Gíslason, G., Eysteinsson, H., Björnsson, G., Harðardóttir, V.: Results of Surface Exploration in the Corbetti Geothermal Area, Ethiopia, *Proceedings*, World Geothermal Congress, Melbourne, Australia (2015), p. 10.

Gottsmann, J., Biggs, J., Lloyd, R., Biranhu, Y., Lewi, E.: Ductility and compressibility accommodate high magma flux beneath a silicic continental rift caldera: Insights from Corbetti caldera (Ethiopia). *Geochemistry, Geophysics, Geosystems* **21** (2020). https://doi.org/10.1029/2020GC008952

Hutchison, W., Mather, T.A., Pyle, D.M., Biggs, J., Yirgu, G.: Structural controls on fluid pathways in an active rift system: A case study of the Aluto volcanic complex. *Geosphere*, **11** (2015), 542–562. https://doi.org/10.1130/GES01119.1

Lavayssière, A., Greenfield, T., Keir, D., Ayele, A., Kendall, J.-M.: Local seismicity near the actively deforming Corbetti volcano in the Main Ethiopian Rift. *Journal of Volcanology and Geothermal Research* **381** (2019), 227–237. https://doi.org/10.1016/j.jvolgeores.2019.06.008

Lloyd, Ryan, Biggs, J., Birhanu, Y., Wilks, M., Gottsmann, J., Kendall, J.-M., Ayele, A., Lewi, E., Eysteinsson, H.: Sustained uplift at a continental rift caldera. *Journal of Geophysical Research: Solid Earth* **123** (2018a), 5209–5226. https://doi.org/10.1029/2018JB015711

Lloyd, R, Biggs, J., Wilks, M., Nowacki, A., Kendall, J.-M., Ayele, A., Lewi, E., Eysteinsson, H.: Evidence for cross rift structural controls on deformation and seismicity at a continental rift caldera. *Earth and Planetary Science Letters* **487** (2018b), 190–200. https://doi.org/10.1016/j.epsl.2018.01.037

Paola, G.M.: Geology of the Corbetti Caldera area (Main Ethiopian Rift Valley). *Bulletin Volcanologique* **35** (1971), 497–506. https://doi.org/10.1007/BF02596970

Shapiro, N.M., Campillo, M.: Emergence of broadband Rayleigh waves from correlations of the ambient seismic noise. *Geophysical Research Letters* **31** (2004), 2004GL019491. https://doi.org/10.1029/2004GL019491

Shi, P., Grigoli, F., Lanza, F., Beroza, G.C., Scarabello, L., Wiemer, S.: MALMI: an automated earthquake detection and location workflow based on machine learning and waveform migration. *Seismological Research Letters* **93** (2022), 2467–2483. https://doi.org/10.1785/0220220071

Wassihun, S., Alemu, A., Nigussie, W., Mickus, K., Keir, D., Wendwesen, S., Wuletawu, H.: Subsurface magmatic structure beneath the nested Awasa–Corbetti caldera complex, Main Ethiopian Rift, as determined from gravity data. *Journal of African Earth Sciences* **233** (2026), 105891. https://doi.org/10.1016/j.jafrearsci.2025.105891

Zhang, X., Roy, C., Curtis, A., Nowacki, A., Baptie, B.: Imaging the subsurface using induced seismicity and ambient noise: 3D Tomographic Monte Carlo joint inversion of earthquake body wave travel times and surface wave dispersion. *Geophysical Journal International* **222** (2020), 1639–1655. https://doi.org/10.1093/gji/ggaa230